Chapter 7

Influence of Nd^{3+} doping in ZnO nanoparticles to enhance the optical and photocatalytic activity

7.1. Introduction:

Nanoscale wide band gap semiconductor is attracting world-wide attention due to enormous improvement in their optical, gas sensing, electrical, magnetic and photocatalytic properties [17, 84, 227]. Waste water, with major amounts of azo dyes, non-fixed dyes and inorganic salts released from textile industries [162-165] pollutes tremendously the environment. Photocatalytic degradation is an effective method to degrade dyes from the waste water [166]. Several metal oxide semiconductors like zinc oxide (ZnO), titanium oxide (TiO_2), tin oxide (SnO_2), tungsten oxide (WO_3) and reduced graphene oxide (RGO) are used as potential photocatalyst for the degradation process. Among these metal oxides, TiO_2 has been widely used due to its cost effectiveness, stable chemical composition and enormous availability [95]. In recent time, it has been discovered that pure and doped ZnO having wide band gap (3.37 eV) and large quantum efficiency act more effectively in deprivation of dyes than TiO_2 [72]. The ZnO based photocatalyst is becoming popular because it has no harmful sideways and is cost effective.

ZnO has a striking feature that it can be improved through many intrinsic defects. Many split in the energy gap can be created through the defects in ZnO structure which enables the compound to act as a potential photocatalyst. Various defects can be induced in ZnO structure by the doping of several metal and non-metal elements [75-77]. Rare-earth ions being optically active [89-91] are potential luminescence centers in doped ZnO nanoparticles and are advantageous for photocatalytic applications. A growing attraction of the researchers has been produced in neodymium, a rare earth group element, due to its potential optical properties in optoelectronic [92] applications. Neodymium ions are used in lasers as gain media. NdYLF (neodymium doped yttrium lithium fluoride), $NDYVO_4$ (neodymium doped yttrium orthovanadate) are some of the materials being used to generate laser beams. Nd^{3+} ion doped ZnO nanoparticles is also emerging as an interesting photocatalytic compound for

degradation of harmful pollutants from the waste water [93, 94]. The photocatalytic activity of Nd-modified ZnO is reported only upto 5% doping. The study was reported on methylene blue (MB) degradation by UV light assisted Nd^{3+} doped ZnO nanoparticles [93]. In this present research work, Nd ion doped ZnO nanopowders have been prepared successfully upto 15% by low cost chemical precipitation method. The outcome of Nd^{3+} doping with its various concentrations on structural and optical properties has been explored. The centre of attention has been put on photocatalytic performance of Nd^{3+} doped ZnO nanocompounds through MB degradation under sunlight.

7.2. Experimental procedures:

7.2.1. Synthesis of pure and Nd-doped ZnO:

The $Zn_{1-x}Nd_xO$ (x = 0.00, 0.03, 0.06, 0.09, 0.12, 0.15) nanoparticles were synthesized through easy chemical precipitation method. Zinc acetate dihydrate [$Zn(CH_3COO)_2 \cdot 2H_2O$] (0.1 M), neodymium chloride ($NdCl_3 \cdot 6H_2O$) (0.1 M) and sodium hydroxide (NaOH) (0.2 M) were used as starting materials and double distilled water was used as solvent. A solution was formed through continuous and vigorous stirring of required amount of zinc acetate, neodymium chloride and sodium hydroxide by a magnetic stirrer. The temperature of solution was maintained at 55 ^oC at the time of stirring. The obtained white precipitate was collected through centrifugation at 6000 rpm. The precipitates were heated at 120 ^oC and finally annealed at 500 ^oC for 2 hour for better stability.

7.2.2. Characterization techniques:

The structural and optical properties of Nd-doped ZnO nanoparticles were investigated by XRD, TEM, UV-Vis absorption and FL characterizations as deliberated in sec 2.2 of chapter 2.

Measurement of photocatalytic activity:

Sunlight driven photocatalytic performance of Nd-doped ZnO nanopowders were examined by MB degradation through the measurement process as described in sec 6.2.2 of chapter 6. The kinetic rate constant (k) of MB degradation was determined from the first-order kinetic eq. $\ln\left(\frac{A_0}{A}\right) = kt$ (7.1)

where A_0 and A is the initial absorbance and absorbance after a particular time interval t respectively and k is the first-order kinetic rate constant. The photocatalytic inspection set-up is displayed in figure 7.1.

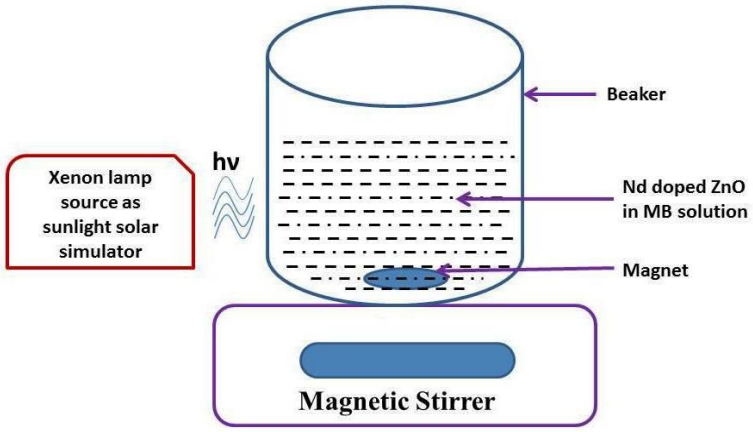

Fig. 7.1. Photocatalytic set-up for MB degradation by Nd-doped ZnO.

7.3. Result and discussions:

7.3.1. XRD:

Crystal structure of pure and Nd^{3+} incorporated ZnO nanocompounds have been inspected by X-ray diffraction study and the XRD patterns of all the compounds are exhibited in figure 7.2. The pattern of all the compounds exhibits peaks at 2θ = 31.9°, 34.5°, 36.4°, 47.7°, 56.7° and 62.9° corresponding to (100), (002), (101), (102), (110), (103) plane which agree with the standard JCPDS file No. 89-0510 of ZnO [233]. Hexagonal wurtzite structure is maintained by all the Nd-doped ZnO samples with space group $P6_3mc$. For higher doping of Nd (15% concentration), two low intense peaks were observed at 26.5° and 45.6° which

signify the presence of excess amount of Nd_2O_3 [296]. Average crystallite size (D) of the nanocompounds have been calculated from Scherrer formula $D = k\lambda / (\beta\cos\theta)$ [207, 277]. The crystallite diameter of the nanoparticles ascribed to highly intense diffraction peaks (100), (002), (101) is presented in table-IX. The lattice parameters for pure ZnO and Nd^{3+} doped ZnO nanoparticles are also presented in the table-IX. The lattice parameters a = b and c have been calculated for that hexagonal crystal structure using the relation

$$\frac{1}{d^2} = \frac{4}{3}\frac{\left(h^2 + hk + k^2\right)}{a^2} + \frac{l^2}{c^2} \tag{7.2}$$

For (100) plane: $a = \frac{\lambda}{\sqrt{3}\sin\theta}$ (7.3)

and for (002) plane: $c = \frac{\lambda}{\sin\theta}$ (7.4)

The value of lattice parameters and average crystallite diameter of Nd-incorporated ZnO nanocompounds for different concentrations are found to be greater than that of pure ZnO nanoparticles. It is worth mentioning here that the ionic radius of Nd^{3+} ion (1.00 Å) is larger than the Zn^{2+} ion (0.74 Å) [96]. The substitution of Zn^{2+} by Nd^{3+} ions in the host ZnO is likely to promote Zn vacancy for charge balancing and also some distortion in the structure as the O^{2-} ions are pulled towards the doped ions [244, 245, 254].

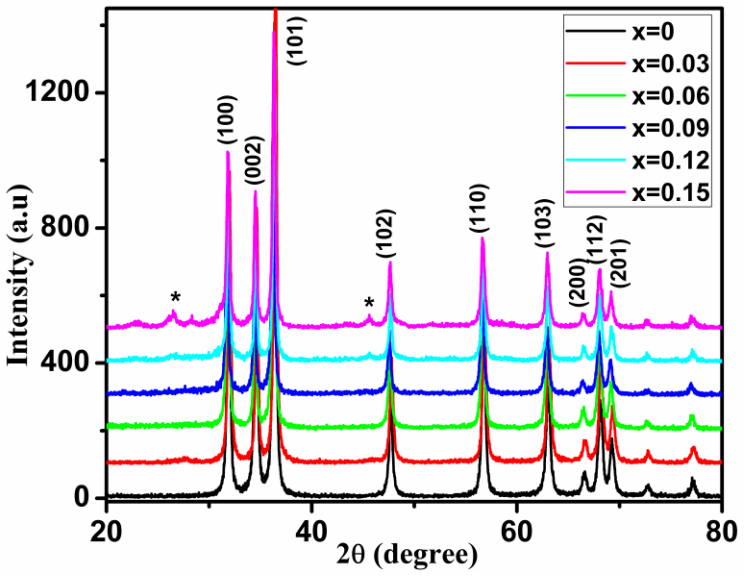

Fig. 7.2. XRD patterns of $Zn_{1-x}Nd_xO$ series.

Table-IX. The average crystallite diameter and lattice parameter of $Zn_{1-x}Nd_xO$ series.

Sample	D (nm) of (100) peak	D (nm) of (002) peak	D (nm) of (101) peak	a in Å	c in Å
ZnO	23.70	21.40	23.90	3.2355	5.1804
$Zn_{0.97}Nd_{0.03}O$	31.37	30.90	26.56	3.2490	5.2016
$Zn_{0.94}Nd_{0.06}O$	31.86	32.29	27.72	3.2509	5.1939
$Zn_{0.91}Nd_{0.09}O$	30.64	31.72	30.88	3.2498	5.2043
$Zn_{0.88}Nd_{0.12}O$	31.93	36.50	32.46	3.2380	5.1866
$Zn_{0.85}Nd_{0.15}O$	28.46	32.29	28.31	3.2391	5.1980

7.3.2. HRTEM and SAED:

HRTEM and SAED of Nd^{3+} doped ZnO nanoparticles have been conducted to gather information on the structural properties and morphology of the nanoparticles. The elemental composition of the nanoparticles also has been investigated through EDX. The TEM and HRTEM photographs of 9% Nd-doped ZnO compounds are exhibited in figure 7.3(a) and 7.3(b) respectively. The TEM photograph indicates the self-assembly with nearly spherical shape (50 nm) of Nd-modified nanocompounds and is greater than the particle size calculated from the XRD results. The lattice spacing determined from HRTEM image is about 0.26 nm which is equal to the interplanar distance of the [002] plane for the sample [194]. A very small segment, identified by square of the entire TEM specimen was used for the SAED study. SAED spectrum of figure 7.3(c) confirms the expected hexagonal arrangement similar to the wurtzite ZnO single crystal. EDX spectrum of $Zn_{0.91}Nd_{0.09}O$ as presented in figure 7.3(d) approve the presence of only Nd, Zn and O elements in the compound. The chemical precipitation method is used to synthesize self-assembled Nd^{3+} doped ZnO nanoparticles with high crystallinity.

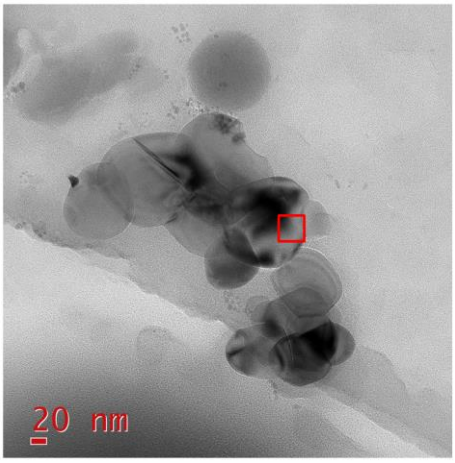

(a)

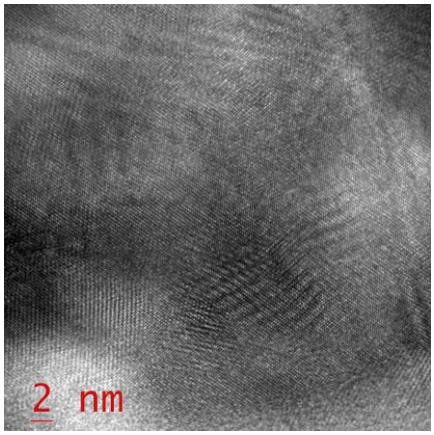

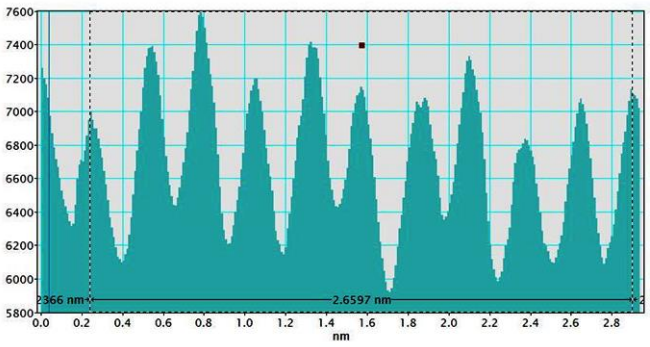

(b)

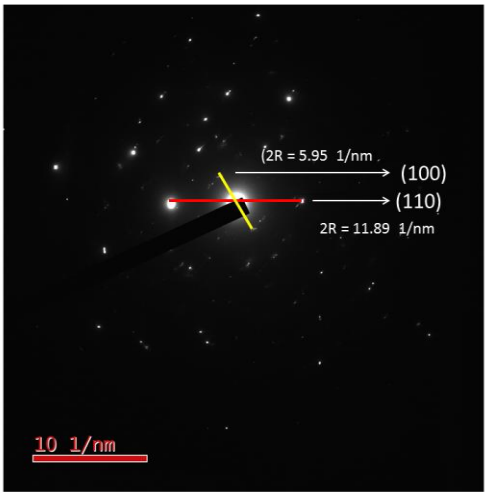

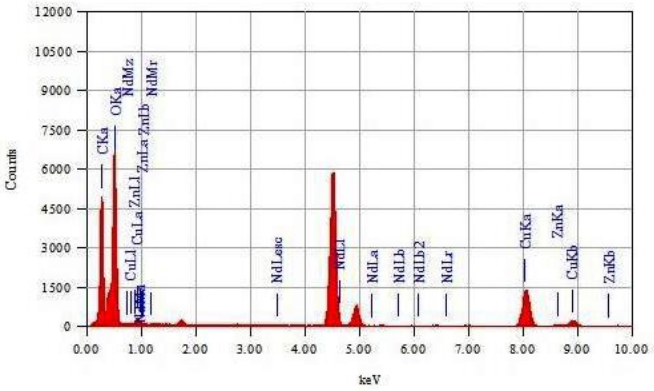

Element	Mass%	Atom%
C	51.98	67.00
O	29.46	28.51
Cu	17.44	4.25
Zn	0.94	0.22
Nd	0.19	0.02
Total	100.00	100.00

(c) **(d)**

Fig. 7.3. **(a)** TEM image, **(b)** HRTEM image, **(c)** SAED pattern, **(d)** EDX pattern of $Zn_{0.91}Nd_{0.09}O$ sample.

7.3.3. UV-Vis absorption:

The UV-Vis absorption property of Nd^{3+} doped ZnO compounds has been investigated between wavelength regions of 200-800 nm and displayed in figure 7.4. The absorption peaks between 372-380 nm have been noticed for pure and doped ZnO nanocompounds. These peaks are attributed to large number of excitons with fundamental absorption [10, 220]. The blue shift observed in absorption spectra is consistent with Burstein-Moss band filling effect [208, 220]. Further in figure 7.4, the absorption peak is highest in case of x = 0.12. As can be seen from the XRD pattern in figure 7.2, the maximum solubility/ miscibility of Nd at the Zn sites is around 12%. Further the particle size of $Zn_{0.88}Nd_{0.12}O$, as can be seen in table-IX, is the largest among all the studied compounds of Nd-doped ZnO. The peak wavelength of the observed absorbance peak is an attribute of the intrinsic band gap of the sample and the intensity depends on the number of states at the valence band maxima. With increase in particle size, the number of states in a band increases (as number of states in a band being equal to 2 times the number of unit cells in the crystallite) and thus enhances the transition probability across the intrinsic band gap. The larger particles thus enhance the absorption peak for the $Zn_{0.88}Nd_{0.12}O$ sample.

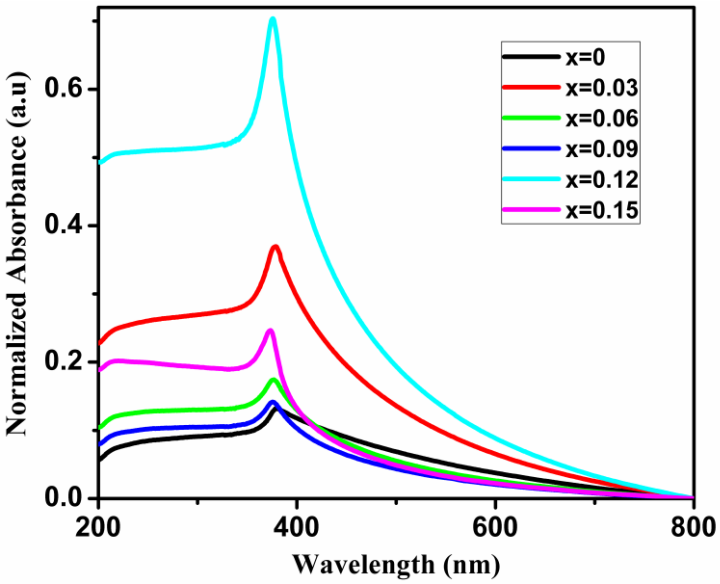

Fig. 7.4. Absorption spectra of $Zn_{1-x}Nd_xO$ series.

7.3.4. Fluorescence:

The FL spectroscopy of $Zn_{1-x}Nd_xO$ nanoparticles for different value of x have been studied at room-temperature with excitation wavelength 325 nm and are presented in figure 7.5. A strong intensity UV peak at 367 nm has been revealed from FL spectra and is ascribed to near-band-edge emission. This type of peak is originated from radiative recombination of electron (e_{CB}^-) and hole (h_{VB}^+) in the conduction and valence band respectively [284]. Two another emission bands between wavelength range 380-427 nm and 464-474 nm have been revealed in the FL spectra for pure and different concentrations of Nd-doped ZnO nanoparticles. Also an emission peak at 412 nm of violet region is observed in FL spectra of 3% Nd-doped ZnO compounds. The violet band 380-427 nm including the emission peak of 412 nm for 3% Nd-doped ZnO correspond to transition of electron from shallow donor levels of natural interstitial zinc (Zn_i) to top of the valence band [210, 215]. Generally in ZnO nanocompounds oxygen vacancy (V_O) and Zn_i are played as donors, while zinc vacancy (V_{Zn}) and interstitial oxygen (O_i) takes a role of acceptors. The weakly intense blue region emission band of 464-474 nm seems to correspond to the transition between the donor level of interstitial zinc (Zn_i) and acceptor level of Zn vacancy [285].

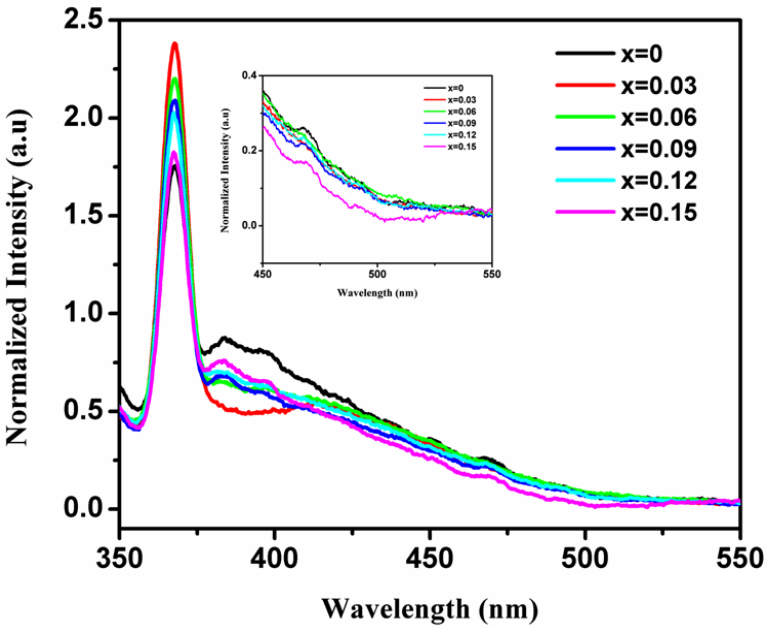

Fig. 7.5. FL spectra of $Zn_{1-x}Nd_xO$ series.

7.3.5. Photocatalytic activity:

Photocatalytic performance of Nd^{3+} doped ZnO nanopowders have been assessed by MB degradation under sunlight and the results are exhibited in figure 7.6(a-f). The rate constant of photocatalytic activity for the different samples with varying Nd^{3+} concentration is being calculated from the slope of the $\ln\left(\frac{A_0}{A}\right)$ vs. time graph presented in figure 7.7. A durable absorption of OH^- ions occurred on the surface of ZnO nanoparticles due to defect states of oxygen vacancies. These OH^- ions may have worked as surface bound traps for the photo-generated holes, which inhibit electron-hole recombination [96]. Photocatalytic reactions are processed through $OH^\bullet$ and $O_2^{\bullet-}$ radicals created on the surface of Nd^{3+} doped ZnO nanosamples. At the time of photocatalysis electron is absorbed by the Nd^{3+} ion and restrain electron-hole recombination as recommended by the following reactions.

$$Nd^{3+} + OH^- \rightarrow Nd^{2+} + OH^\bullet \quad (7.5)$$

$$OH^\bullet + MB \rightarrow Degraded\ Products \quad (7.6)$$

$$Nd^{3+} + e^- \rightarrow Nd^{2+} \quad (7.7)$$

$$Nd^{2+} + O_2 \rightarrow Nd^{3+} + O_2^{\bullet-} \quad (7.8)$$

$$O_2^{\bullet-} + MB \rightarrow Degraded\ Products \quad (7.9)$$

The above mentioned reactions are generated by $O_2^{\bullet-}$ superoxide ions. The increase in doping concentration of Nd^{3+} ion assists photonic absorption as electrons are being captured by these ions to diminish electron-hole recombination [93]. The calculated rate constants for pure and Nd^{3+} doped ZnO nanoparticles are 0.008, 0.012, 0.017, 0.021, 0.03, 0.038 min^{-1} respectively [297]. High value of band gap energy fruitfully affected the photocatalytic activity due to higher redox potential of photo-generated electron-hole pairs [85, 286]. Hence Nd-doped ZnO nanocomposites possess improved photocatalytic activity. Here the photocatalytic performance has been controlled by both the band gap energy and the defect

states. As Nd^{3+} doping creates more surface defects and a space charge layer is formed on the surface which can transmit the photo-induced electrons and holes into surface defects [287]. This process executes the dynamics responsible for the improvement of photocatalytic performance for the modified ZnO nanocomposites. In 2018 a survey on methylene blue (MB) degradation has informed that the photocatalytic kinetic rate constant of ZnS–TiO_2/RGO composites is 0.019 min^{-1} [166]. The kinetic rate constant of iron modified ZnS nanocomposite has been reported to be 0.0035 min^{-1} [298]. In 2012, a report on MB degradation has exhibited the kinetic rate constant of Ag doped TiO_2 photocatalyst as 0.027 min^{-1} [299]. Further in 2018, the photocatalytic kinetic rate of ZnS for MB degradation is reported to have a value of 0.02 min^{-1} [300]. The maximum kinetic rate for ZnS-CdS mixture and TiO_2 are reported at 0.0036 min^{-1} and 0.0033 min^{-1} respectively [301, 302]. Here, photocatalytic rate constant for degradation of MB with the help of self-employed Nd^{3+} doped ZnO nanoparticles have been accomplished at 0.038 min^{-1} which is much higher than the earlier reported values for Zn based compounds. Further, the photocatalytic performance increases with Nd ion concentration because the separation efficiency of the electron-hole pairs for the doped ZnO nanomaterials seems to increase with increasing the Nd^{3+} doping concentration. Hence, the surface defect is a significant factor for the photocatalytic activity of Nd^{3+} doped ZnO nanoparticles which is also conveyed previously through FL characterization of these nanoparticles. Fluorescence emission intensity and photocatalytic performance are strongly allied with each other as the emissions are ascribed to the recombination of photo-generated charge carriers [288-290]. Excitonic emission intensity of $Zn_{0.85}Nd_{0.15}O$ has become smaller and the photocatalytic activity is larger than other doped samples. In the same way, $Zn_{0.97}Nd_{0.03}O$ has given most intense fluorescence peak and smaller photocatalytic activity because of rapid recombination of photo-induced charge carriers. The response of pure ZnO nanoparticles both in photocatalytic performance and

excitonic emission is smaller compared to Nd^{3+} doped ZnO nanoparticles because of its relatively lower band gap. Hence it may be concluded that the photocatalytic effect in Nd^{3+} doped ZnO compound depend on both the band gap and the surface defects.

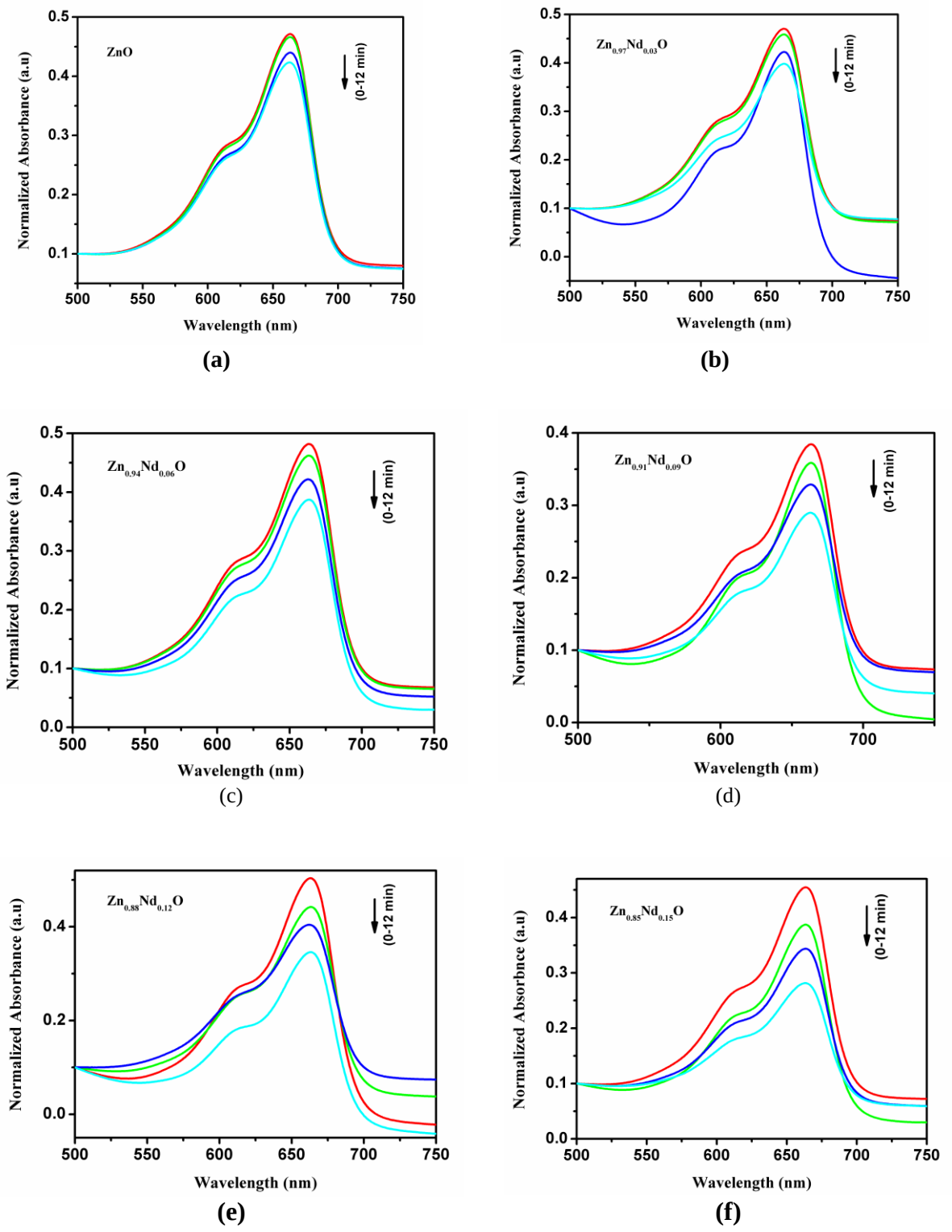

Fig.7.6. Photocatalytic degradation of **(a)** pure ZnO **(b)** $Zn_{0.97}Nd_{0.03}O$ **(c)** $Zn_{0.94}Nd_{0.06}O$ **(d)** $Zn_{0.91}Nd_{0.09}O$ **(e)** $Zn_{0.88}Nd_{0.12}O$ and **(f)** $Zn_{0.85}Nd_{0.15}O$.

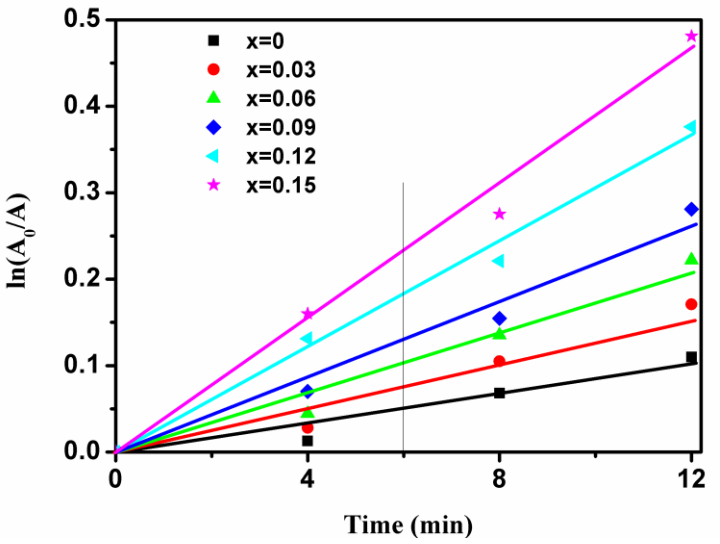

Fig. 7.7. Kinetic study of methylene blue degradation.

7.4. Conclusion:

The pure and neodymium incorporated ZnO nanopowders are synthesized through an easy and inexpensive chemical precipitation technique. X-ray characterization endorses the successful doping of Nd^{3+} ion at Zn^{2+} sites of wurtzite ZnO matrix. The average crystallite diameter as has been realized from TEM image is about 50 nm. The HRTEM exhibits that the nanosized compounds is found to have single crystalline nature with the direction perpendicular to the (002) plane is the preferred growth direction. Nd^{3+} doped ZnO nanoparticles explore more intense excitonic emission at 367 nm compared to pure one. A superior photocatalytic activity has been documented for Nd^{3+} doped ZnO nanoparticles. 15% doping of Nd^{3+} ion in ZnO nanoparticles raises the photocatalytic rate by 375% and is found to be much higher than all Zn based compounds. Based on the advanced optical properties and photocatalytic performance, Nd^{3+} ion incorporated ZnO nanocompounds can be recommended as advance nanomaterials for effective sunlight-irradiated photocatalytic reaction, self-cleaning and photovoltaic applications.

[Results of this work have been published in Mater. Res. Express 6 (2019) 065031. (Ref. 297)]